International Journal of Pharmaceutics 644 (2023) 123353

Contents lists available at ScienceDirect

International Journal of Pharmaceutics

journal homepage: www.elsevier.com/locate/ijpharm

Phase transitions of aqueous solutions of Pluronic F68 in the presence of Diclofenac Sodium

Nicola Antonio Di Spirito [a], Nino Grizzuti [a], Mosè Casalegno [b,*], Franca Castiglione [b,*], Rossana Pasquino [a,*]

[a] DICMaPI, Università degli Studi di Napoli Federico II, P. le Tecchio 80, 80125 Napoli, Italy
[b] Dipartimento di Chimica, Materiali e Ingegneria Chimica "G. Natta", Politecnico di Milano, via Mancinelli 7, I-20131 Milano (MI), Italy

ARTICLE INFO

Keyword:
Pluronics
Diclofenac Sodium
Drug delivery
Phase diagram
Rheology
NMR

ABSTRACT

In recent years, advancements in bioengineering and materials science have witnessed increasing interest in synthetic polymers capable of fulfilling various applications. Owing to their distinctive properties, Pluronics can be used as nano-drug carriers, to deliver poorly water-soluble drugs, and as model systems to study colloidal science by tuning amphiphilic properties. In this work, we investigated the effect of diclofenac sodium on the self-assembly and thermoresponsive crystallization of Pluronic F68 in water solutions, by employing experimental rheology and Nuclear Magnetic Resonance (NMR). We built a complete phase diagram as a function of temperature and concentration for 45 wt% Pluronic F68 with various amounts of diclofenac sodium in water. The morphological transitions were followed as a function of temperature via linear rheology. We extrapolated the transition temperatures – identifying distinct phases – as a function of the drug concentration and proposed an empirical model for their prediction. NMR analysis provided further information on the structural characteristics of the systems, shedding light on the interactions between F68 and diclofenac sodium. Although dealing with a pharmaceutical salt, the study is focused on a colloidal system and its interaction with a binding molecule, that is of general interest for colloidal science.

1. Introduction

The last few decades have seen an increasing effort in the development of products and materials with high degree of biocompatibility and tunable properties. Biomaterials and biocompatible synthetic polymers are of paramount importance in many biomedical areas, ranging from drug delivery, tissue engineering and pharmaceutics, to three-dimensional (3D) printing (Biondi, 2008; Zarrintaj, 2018; Kim, 2018; Smeraldo, 2021; Salerno and Netti, 2021). Particular attention is given to biomimicking scaffolds, as they can be adopted as bioengineered supports in tissue regeneration (Chubinskaya, 2019; Zarrintaj, 2017), and self-assembled carriers to deliver drugs into human body (Mohammadi, 2017).

Pluronics, also known as Poloxamers, are a class of synthetic polymers with unique properties used in a wide range of applications (Zarrintaj, 2020), such as cell cultures (Clincke, 2011), pharmaceutics (Dumortier, 2006), 3D bioprinting (Suntornnond, 2017), tissue engineering (Gioffredi, 2016), and drug delivery (Batrakova and Kabanov, 2008; Oshiro, 2014). Biocompatibility, thermosensitivity and self-assembling behavior (Quintans-Júnior, 2018; Gjerde, 2018; Alexandridis et al., 1994) make them leading materials in the field of drug delivery and nanomedicine (Yang and Alexandridis, 2000; Rahdar et al., 2018).

Pluronics are nonionic amphiphilic copolymers with a triblock structure made of a central hydrophobic unit of poly(propylene oxide) (PPO) bordered by two hydrophilic segments of poly(ethylene oxide) (PEO) (Herzberger, 2016), in a PEO-PPO-PEO sequence.

Pluronics are commercially available in different types, as their total molecular weight and properties can be tailored by tuning the length of PPO and PEO chains. The diagram where the various Pluronics are catalogued is called Pluronic grid (Newman et al., 1998). A specific Pluronic is conventionally named with an alphanumeric code composed of a letter, which refers to its physical form at room temperature (L for liquid, P for paste, and F for flakes), and two or three digits, which

* Corresponding authors.
E-mail addresses: nicolaantonio.dispirito@unina.it (N.A. Di Spirito), nino.grizzuti@unina.it (N. Grizzuti), mose.casalegno@polimi.it (M. Casalegno), franca.castiglione@polimi.it (F. Castiglione), r.pasquino@unina.it (R. Pasquino).

https://doi.org/10.1016/j.ijpharm.2023.123353
Received 7 June 2023; Received in revised form 25 August 2023; Accepted 26 August 2023
Available online 28 August 2023

indicate molecular weight and composition.

Pluronics can be solubilized in many polar and nonpolar solvents. Depending on Pluronic type, polymer concentration, solvent, and temperature, Pluronic solutions present a different phase behavior (Bedrov et al., 2006; Artzner, 2007; Denkova, 2011; Wanka et al., 1994; Pasquino, 2019; Costanzo, 2021). The properties and the phase diagrams of numerous Pluronics in aqueous solutions have been already examined in the past (Artzner, 2007; Wanka et al., 1994; Pasquino, 2019; Costanzo, 2021; Mortensen, 2001; Alexandridis et al., 1996; Meng, 2006; Gaisford et al., 1997). Scientific works on Pluronics often rely on sophisticated techniques, such as scattering, fluorescence, NMR, etc., to obtain the phase diagrams and describe the micellization process and the phase transitions (Gjerde, 2018; Artzner, 2007; Wanka et al., 1994; Costanzo, 2021; Ray et al., 1832), often coupled to rheological tools to support the description of the microstructural evolution of the system.

An important highlight of Pluronic solutions is their temperature dependent, self-assembly behavior (Bodratti and Alexandridis, 2018). Some of them reversibly form a solid-like structure at higher temperatures and they are, as such, used in many biomedical applications to manufacture hydrogels (Chung, 2014; Chen, 2013). For example, Pluronic F68 in water experiences a reversable thermal crystallization with increasing temperature (Wanka et al., 1994; Costanzo, 2021; Wu, 2006). More specifically, Pluronic F68 in water can form three distinct phases: individual unimers, disordered spherical micellar structures, and a body-centered cubic (BCC) crystalline phase. At temperatures and concentrations below a critical micellar temperature (CMT) and a critical micellar concentration (CMC), the polymer is homogeneously dissolved in solution as individual unimers. Above the CMT and CMC, the single Pluronic molecules aggregate and form micellar structures. After micellization, the hydrophobic PPO blocks occupy the core of the micelles, whereas hydrophilic PEO segments are arranged on the micellar shell, in order to screen the negative interactions between the PPO segments and the solvent, increasing the stability of the micelles. A further temperature increase determines a swifter reduction in hydrophilicity of the PPO segment with respect to the PEO tails. The micellar structures, in turn, begin to act as hard bodies, causing a change in the microstructure and rheology of the system, generating a thicker solution. At high temperatures, Pluronic F68 solutions take on the appearance of soft solids. Therefore, a reversible liquid-to-solid transition depicts the passage from a viscoelastic liquid to a soft solid.

Thanks to their peculiar transitions, Pluronics carved a space in the subcutaneous drug delivery world (Liu, 2007; Zhang, 2010; Müller, 2015; Torchilin, 2001). The use of rheology to investigate the viscoelastic properties of the materials and the transition temperatures helps in understanding the effects of drugs on the rheological and phase behavior of Pluronics. Dorn et al. (Dorn et al., 1985) first showed interest in the formulation of polymeric micelles-drug systems. Sharma and Bhatia (Sharma and Bhatia, 2004) analyzed the effect of two hydrophobic drugs, naproxen and indomethacin, on the structure, assembly and transition temperature of Pluronic F127. They used Dynamic Light Scattering (DLS) to determine the CMC, and Small-Angle Neutron Scattering (SANS) to study the micellar structure. They found that these hydrophobic drugs determine a decrease of both micellar sizes (radii of the micelle core and corona) and micelles aggregation number, and a decrease of the transition temperature. Sahu et al. (Sahu, 2011) dealt with the incorporation of curcumin, a diarylheptanoid with therapeutic potential, in Pluronic F12 and F68, to analyze its *in vitro* release. Basak and Bandyopadhyay (Basak and Bandyopadhyay, 2013) embedded three different drugs (ibuprofen, aspirin and erythromycin) in the hydrophobic cores of Pluronic F127 micelles, analyzed the shape and the size distribution of micelles – with and without drugs – by means of cryo-scanning electron microscopy and DLS, and investigated the effects of drug hydrophobicity, temperature and pH. They observed the increase of the micelle mean hydrodynamic radius with decreasing temperature. Scherlund et al. (Scherlund et al., 2000) studied the micellization and transition processes in Pluronic systems containing local anesthetics – i.e., lidocaine and prilocaine – by means of different and complementary techniques. Furthermore, they investigated the effect of cosolutes, such as salts and hydrophobic molecules, PH, and block copolymer ratio, on the phase transition temperatures. Wu et al. (Wu, 2006) analyzed the influence of salt on the phase behavior of Pluronic F68 in water through viscosity measurements, microscopy and Small-Angle X-ray Scattering (SAXS), and experimentally built a phase diagram of Pluronic F68 with 1 M sodium chloride. Russo et al. (Russo et al., 2020) adopted rheology and *in vitro* studies to investigate the system containing Pluronic F127 and diclofenac sodium. They observed an increasing of transition temperature with increasing diclofenac sodium concentration. Later, they examined the impact of salt form (diclofenac sodium, potassium, epolamine, and diethylamine) on the transition and drug delivery behavior of Pluronic F127-based structures, showing that – as observed in their previous investigation – the transition temperature increases with increasing diclofenac concentration, for all salt forms (Russo et al., 2022).

NMR Spectroscopy techniques provide a natural complement to rheology in the analysis of drug delivery systems (Scherlund et al., 2000). So far, 2D High Resolution (HR) and High Resolution Magic Angle Spinning (HR-MAS) NMR Spectroscopy has been successfully used to obtain information on the structure, dynamics, and local environment of interacting species, e.g., drug-polymers, multicomponent supramolecular gels (Fiorati, 2020), or host–guest systems (Sayed, 2021). The magnitude of chemical shift perturbations can be used to determine changes in the local electronic environment caused by intermolecular interactions between drug molecules and surfactants or binding sites.

Meanwhile, Pulse Field Gradient Spin Echo (PGSE) methodologies, which allow for the determination of self-diffusion coefficients and T_2 relaxation times, has proven to provide valuable information about drug diffusion mechanism in soft systems (Scherlund et al., 2000; Casalegno et al., 2019). Applications to pluronic-based systems have so far focused on the micellization process (Shaikhullina, 2020), and the incorporation of drug molecules into micelles (Saveyn, 2009). Thanks to specifically designed numerical approaches, such as the q-space approach (Cory and Garroway, 1990; Callaghan et al., 1988), PGSE-NMR is especially well suited to study the translational dynamics of small molecules in heterogeneous systems. Here, either due to intermolecular interactions or physical confinement, solute diffusion can be expected to deviate from ordinary, Gaussian diffusion, which is commonly expected in isotropic and homogeneous media.

In this work we present an experimental investigation on the phase behavior of aqueous solutions of Pluronic F68 (alias Poloxamer 188) and diclofenac sodium. Due to the presence of heteroatoms and aromatic moieties, diclofenac is quite soluble in several organic solvents; however, it is poorly soluble in water, thus limiting its efficacy (Žilnik, 2007). Thus, it is often combined with versatile amphiphilic carriers. We adopted distinct experimental techniques to provide a full description of both the macroscopic flow properties and microstructure of the systems. Specifically, we exemplified the usefulness of rheology and NMR Spectroscopy to explore the influence of diclofenac sodium on the self-assembly and crystallization properties of Pluronic F68 in water.

2. Materials and methods

2.1. Materials

The amphiphilic copolymer investigated in this work is Pluronic F68 (Sigma-Aldrich, St. Louis, MO). It owns a molecular weight of 8,350 g/mol, with 80% of PEO. Diclofenac sodium salt (Tokyo Chemical Industry Co., TYO, JP, molecular weight = 318 g/mol) is the drug used in our research. Diclofenac sodium is a therapeutic drug belonging to Non-Steroidal Anti-Inflammatory Drug (NSAID) class, advocated for treatment of pain and inflammatory conditions (Scholer, 1986). The substance, whose chemical structure is shown in scheme 1, is a salt of a weak acid with a pKa of 4.

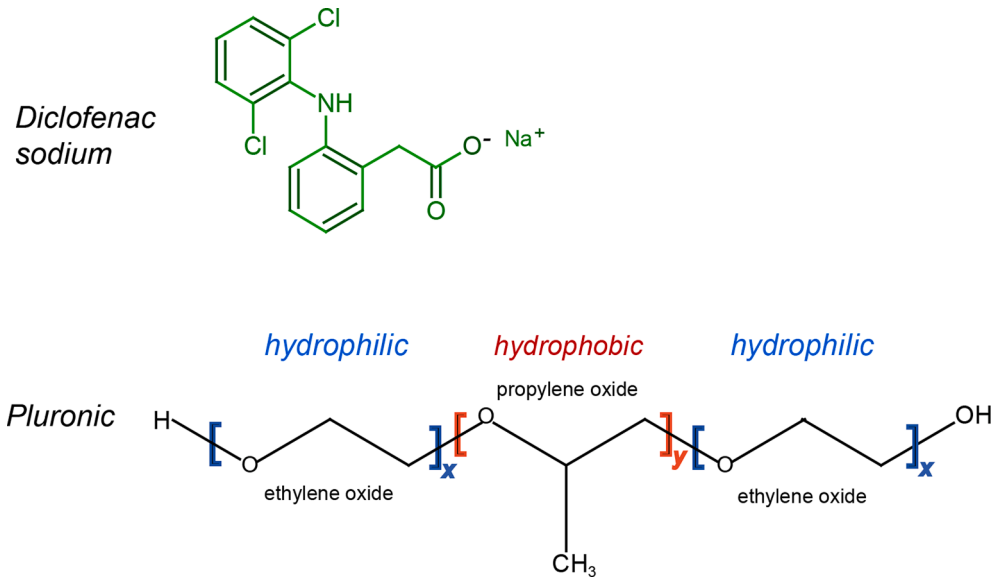

Scheme 1. Chemical structures of diclofenac sodium salt and Pluronics (F68: x = 82, y = 31).

Aqueous solutions of 45 wt% Pluronic F68 were prepared at room temperature by dispersing the polymer in cold water (5 °C) (Schmolka, 1972). Through magnetic stirring, vortices were created, and the polymer was gradually introduced to guarantee a homogeneous distribution. The aqueous Pluronic solutions were stored at 5 °C for a few days, and periodically subjected to magnetic stirring, to allow for their complete dissolution. Then, diclofenac sodium was added to the mixtures. The pluronic-diclofenac solutions were shaken by means of a tilting table for 48 h. We prepared various water solutions with a fixed Pluronic F68 concentration (45 wt%) and different diclofenac sodium contents (0–300 mM).

2.2. Experiments

2.2.1. Rheology

The rheological properties of the samples were experimentally studied by using a rotational stress-controlled rheometer (DHR-2, Discovery Hybrid Rheometer, TA Instruments, USA), equipped with 40 mm sandblasted parallel plates. The temperature was controlled via a Peltier unit. Temperature ramp tests – at constant rates of 0.5 and 5 °C/min – were performed at 10 rad/s, to follow the transition temperatures. Moreover, the sample viscoelasticity was studied by frequency sweep tests in the linear regime at lower and higher temperatures. Strain sweep tests were performed to guarantee the linear viscoelastic regime in the dynamic tests. A value of strain equal to 0.1% was used for all the experiments. During all rheological measurements, the rim of the samples was surrounded by low viscosity silicone oil to prevent water evaporation.

In particular, we adopted the following protocol:

- samples loading at 5 °C;
- waiting 5 min for thermal equilibrium;
- performing a time sweep test for 10 min;
- performing a frequency sweep test at 5 °C;
- heating at a constant rate until attaining the liquid-to-solid transition;
- performing a frequency sweep test at the highest temperature;
- cooling up to 5 °C at the same rate of the heating ramp;
- performing a further frequency sweep test at 5 °C to check the process reversibility.

The visual investigation of the diclofenac sodium solubility at the highest concentration was performed by means of an Anton Paar rheo-optical tool (P-PTD 200/GL). 50 mm transparent glass plates combined with a simple camera (Digital Eye 250) and a Peltier unit to control temperature were used to visualize solution homogeneity and stability. Specifically, heating and cooling temperature ramp tests from 5 °C to 30 °C at 0.5 °C/min were performed, with time sweeps at 30 °C lasting 1 h after the heating cycle, and at 5 °C lasting 11.7 h after the cooling cycle.

2.2.2. NMR

2.2.2.1. Data acquisition. Proton Nuclear Magnetic Resonance (^{1}H NMR) was employed to analyze the aqueous Pluronic samples without (0 mM) and with (100 and 300 mM) diclofenac sodium and a dilute (15 mM) solution of diclofenac sodium in D_2O. The ^{1}H HR NMR data were acquired on a Bruker NEO 500 console (11.74 T) equipped with a direct observe BBFO (broadband including fluorine) iProbe and a variable-temperature unit (^{1}H resonance frequency of 500.13 MHz). Self-diffusion coefficients were measured by pulsed gradient spin echo (PGSE) experiments applying sine-shaped pulsed magnetic field gradients along the z-direction up to a maximum strength of G = 48.15 G cm^{-1}. The diffusion experiments were performed using the bipolar pulse longitudinal eddy current delay (BPP-LED) pulse sequence shown in figure SI1 (Wu et al., 1995). The pulse gradients were incremented from 2 to 95% of the maximum gradient strength in a linear ramp with 24–32 steps. For each experiment, the duration of the magnetic field pulse gradients (δ) and the diffusion times (Δ) were optimized to obtain 95% signal attenuation at the last step experiment. δ values were 3.0–6.0 ms range, while Δ values were 0.05–0.4 s long. All experiments were performed in the temperature range 5–45 °C with 16 scans, a relaxation delay D1 of 10 s and sweep width of 10 ppm. The two-dimensional homonuclear ^{1}H–^{1}H NOESY correlation experiments were recorded with a sweep width of 10 ppm, 8 scans for each of the 512 increments (F1), 4096 data points (F2), a mixing time of 300 ms and T = 5–25 °C. The HR-MAS experiments were performed with a dual ^{1}H/^{13}C high-resolution magic angle spinning (HR-MAS) probe head for semisolid samples. The sample was loaded into 4 mm ZrO_2 rotor (12 μL volume). The spectra were acquired at a spinning rate of 4 kHz, sweep width of 10 ppm, 8 scans and T = 70 °C. The diffusion data were acquired with δ = 6.0 ms, Δ = 0.09 s and a linear ramp gradient of 24 steps.

2.2.2.2. PGSE-NMR diffusion data analysis. PGSE-NMR enables the

study of molecular diffusion through the collection of the signal intensity resulting from the application of a pulsed magnetic field gradient. The attenuation of signal intensity associated with the probed nuclei can be written as follows:

$$I(\mathrm{q},\mathrm{t}) = \mathrm{I}(0,\mathrm{t})\cdot e^{-\frac{1}{2}q^2\langle z^2(t)\rangle} \quad (1)$$

with t the effective time between encoding and decoding gradients, q the reciprocal space coordinate, defined as $q = (\delta\gamma g)/2\pi$, γ is the magnetogyric ratio of the observed nucleus, g is the field gradient and δ is the gradient pulse. According to the Stejskal-Tanner equation (Stejskal and Tanner, 1965) $t = \Delta - \delta/3$. To evaluate our data with respect to Δ, we simplified the previous equation as $t = \Delta$.

The quantity in square brackets, $\langle z^2(t)\rangle$, represents the mean squared displacement (MSD) along the magnetic field axis z, which, in the case of Fickian diffusion, changes linearly over time:

$$\langle z^2(t)\rangle = 2D\cdot t \quad (2)$$

where D is the diffusion coefficient. We note that, due to the small magnitude of δ, this simplification had negligible effects on our fitting results. A further connection between signal intensity and diffusion properties can be established considering the relationship between the displacement probability distribution (PDF) of the probed nuclei, $G(z,t)$, and the signal intensity (Callaghan et al., 1988; Cohen and Assaf, 2002; Cory and Garroway, 1990):

$$I(\mathrm{q},\mathrm{t}) = \int_{-\infty}^{+\infty} G(\mathrm{z},\mathrm{t})\cdot e^{-iqz}\mathrm{dz} \quad (3)$$

The displacement probability distribution may, in principle, assume different forms. For species diffusing in isotropic media $G(z,t)$ can be written as a Gaussian function, e.g.:

$$G(\mathrm{z},\mathrm{t}) = \mathrm{I}(0,\mathrm{t})\frac{1}{\sqrt{4\pi\mathrm{Dt}}}e^{-\frac{z^2}{4\mathrm{Dt}}} \quad (4)$$

Replacing Eq. (4) in Eq. (3) leads to:

$$I(\mathrm{q},\mathrm{t}) = \mathrm{I}(0,\mathrm{t})\cdot e^{-q^2\mathrm{Dt}} \quad (5)$$

The latter may also be obtained by replacing Eq. (2) into Eq. (1), demonstrating that a Gaussian PDF also implies that the diffusion conforms to Fick's laws (Fick, 1855). As already mentioned Gaussian diffusion generally occurs for species diffusing in isotropic media, such as pure liquids, in which cases the diffusion is termed free and unrestricted.

As far as Gaussian diffusion is considered, the diffusion coefficient can be obtained in a straightforward way, by fitting the signal intensity of a single PGSE-NMR measure at a given diffusion time (see Eq. (5), or by means of linear regression over a set of measurements collected at different times. In the following, we shall use these approaches to fit our NMR data.

Meanwhile, since deviations from the Gaussian behaviour have recently been reported in heterogeneous soft systems (Guan et al., 2014; Tang et al., 2015; Stempfle, 2014; Bertz, 2013; Chakraborty, 2019; Kurtuldu, et al., 2011; Thorneywork, 2016), we shall also adopt a complimentary approach which allows for the detection of non-Gaussian diffusion patterns. This method, called Gaussian deconvolution (GD), has been exploited in particle-tracking experiments (Wang, 2012; Wang, et al., 2009), to model $G(z,t)$. Hereafter, for the first time to our knowledge, this approach is directly applied to model NMR signal intensities.

The method assumes that diffusion may result from the superposition of different, yet Gaussian, diffusive processes. Accordingly, the displacement distribution function (Eq. (4) can be written as a linear combination of Gaussian functions associated with different diffusion coefficients. Taking into account for the relationship between $G(z,t)$ and $I(q,t)$, the same approach can be applied to signal intensity, so to obtain the distribution of diffusion coefficients associated to the probed molecules. More specifically, the average signal intensity can be written as:

$$I(q,t) = I(0,t)\int P(D)e^{-\frac{1}{2}q^2D\cdot t}dD \quad (6)$$

where $P(D)$ is a probability distribution function.

In this work, we implemented the Lucy-Richardson algorithm (Lucy, 1974; Richardson, 1972) to obtain a numerical approximation of $P(D)$ for each NMR experiment. Details about its implementation, the calculation of the average diffusion coefficient and its uncertainty, are given in the SI. Single-Gaussian fitting of signal intensity was addressed by means of the Levenberg-Marquardt algorithm (Levenberg, 1944; Marquardt, 1963), as implemented in the Gnuplot software (Gnuplot, 2023).

3. Results and discussion

3.1. Rheology

We experimentally studied the rheological and phase behavior of aqueous solutions containing 45 wt% Pluronic F68 and various amounts of diclofenac sodium, as previously reported.

Figs. 1 and 2 display temperature ramp tests (at 10 rad/s) performed on Pluronic samples with a drug content between 0 and 100 mM (see legend for details), at 5 and 0.5 °C/min, respectively. The complex modulus, G*, is reported as a function of temperature during the heating and cooling steps.

Figs. 1 and 2 reveal that all samples undergo a reversable thermal phase transition, with a hysteresis loop. The heating/cooling cycles exhibit two characteristic transition temperatures in correspondence of the inflection points of the complex modulus: a liquid-to-solid transition temperature (T_{LS}), corresponding to the transition during heating, and a solid-to-liquid transition temperature (T_{SL}), representative of the transition during cooling. At low temperatures, the systems present low values of G*. The increase of temperature causes a hasty growth of G* by many orders of magnitude, resulting in a solid-like behavior. The transition temperatures increase with increasing diclofenac content (Yong, 2001). In Fig. 3, we report the transition temperatures as a function of diclofenac sodium concentration (c_{DS}), as obtained from the temperature ramps of Figs. 1 and 2.

The use of different heating/cooling rates allows to assess the influence of the ramp rate on the transition temperatures. Figs. 1-3 indicate the trend of the hysteresis cycles breadth to shrink with decreasing ramp rate. As described by Costanzo et al. (Costanzo, 2021), T_{LS}

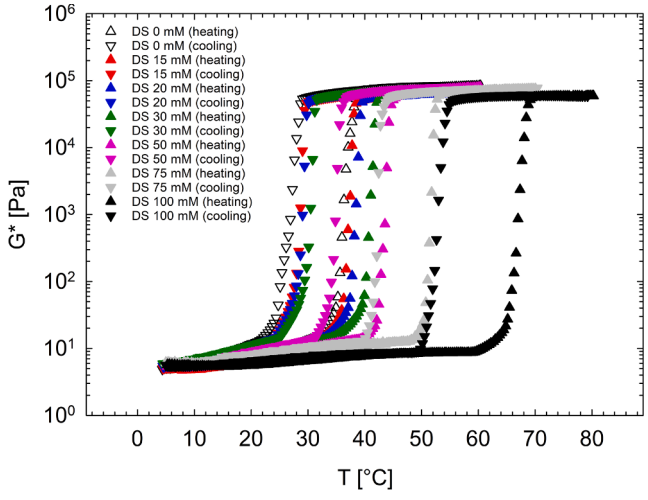

Fig. 1. Complex modulus vs temperature for the 45 wt% Pluronic F68 aqueous solutions with various amounts of diclofenac sodium (indicated with DS in the legend). Ramp rate: 5 °C/min.

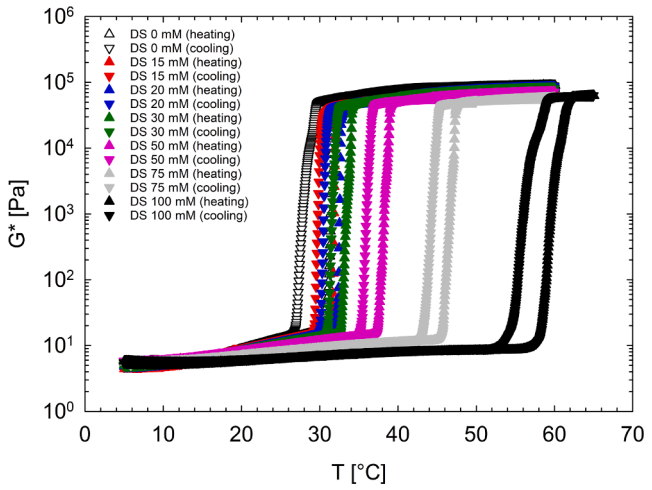

Fig. 2. Complex modulus vs temperature for the 45 wt% Pluronic F68 aqueous solutions with various amounts of diclofenac sodium (indicated with DS in the legend). Ramp rate: 0.5 °C/min.

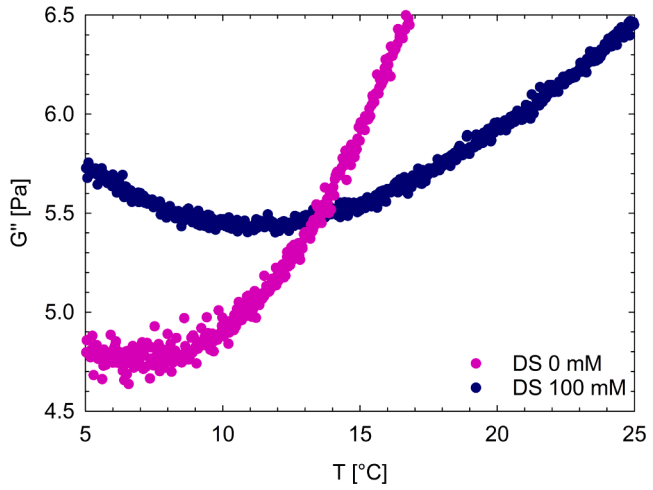

Fig. 4. Loss modulus vs temperature for the 45 wt% Pluronic F68 aqueous solutions with 0 and 100 mM diclofenac sodium (indicated with DS in the legend). Ramp rate equal to 0.5 °C/min.

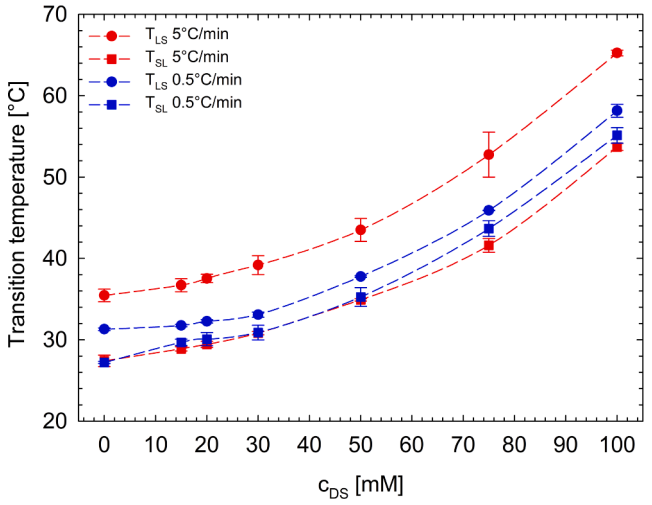

Fig. 3. Transition temperatures as a function of diclofenac sodium concentration. The error bars are evaluated as standard deviations of multiple experiments.

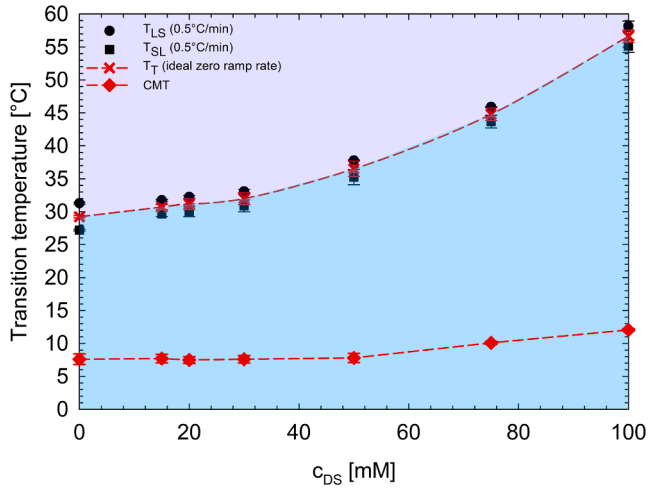

Fig. 5. Ideal transition temperatures and CMTs as a function of diclofenac sodium concentration.

coincides with T_{SL} at an ideal zero ramp rate. We estimated this ideal transition temperature, T_T, at various drug concentrations as the arithmetic average of T_{LS} and T_{SL} measured at 0.5 °C/min, which is the lowest investigated ramp rate, as shown in Fig. 5.

As described by Costanzo et al. (Costanzo, 2021), the micellization temperature of such systems can be detected by magnifying the temperature ramp tests in the low-temperature range. In particular, the CMT can be assumed to be the temperature at which the loss modulus has its minimum. As an example, Fig. 4 shows the loss modulus as a function of temperature in the low-temperature range for the sample without drug and the one with 100 mM diclofenac sodium.

The CMT – macroscopically identifying the transition from single unimers to a conspicuous number of spherical micelles – is equal to 7.6 ± 0.8 °C for the sample without drug (Costanzo, 2021), and 12.1 ± 0.2 °C for the sample with 100 mM diclofenac sodium. We report in Fig. 5 the CMT for all the investigated samples.

Fig. 5 represents the rheological phase diagram as a function of temperature and diclofenac sodium concentration for the aqueous solutions containing 45 wt% Pluronic F68 and various amounts of diclofenac sodium. The transition temperatures at an ideal zero ramp rate describe the passage from the liquid phase (light blue area) to the crystalline one (light purple area); the CMTs describe the transition from unimers to micellar aggregates.

The frequency sweeps of the pluronic-drug systems at various temperatures were also measured. As an example, the linear viscoelastic properties of the sample at 50 mM diclofenac sodium are described in Fig. 6. In Fig. 6a, the frequency response at high temperature (70 °C) is reported, showing a well-defined crossover (i.e., the inverse of which marks a very long relaxation time) and a pronounced elastic behavior. Fig. 6b reports the dynamic frequency sweep tests at low temperature (5 °C), before and after the temperature ramp test. The perfect overlap of the two frequency responses indicates the process reversibility. In this case, the trend and the absolute values of the viscoelastic moduli reveal a liquid-like behavior in the entire frequency range.

When moving to diclofenac sodium concentrations larger than 100 mM we discover a completely different, unexpected rheological behavior, which is liquid-like in the entire investigated temperature range. Fig. 7 describes the loss modulus, G", as a function of temperature upon heating for the 45 wt% Pluronic solutions with 200 mM and 300 mM diclofenac sodium. In this case, a progressive, monotonic reduction in G" is visible in the whole temperature range (5–95 °C) for both samples, suggesting the absence of a minimum and, as a consequence, of

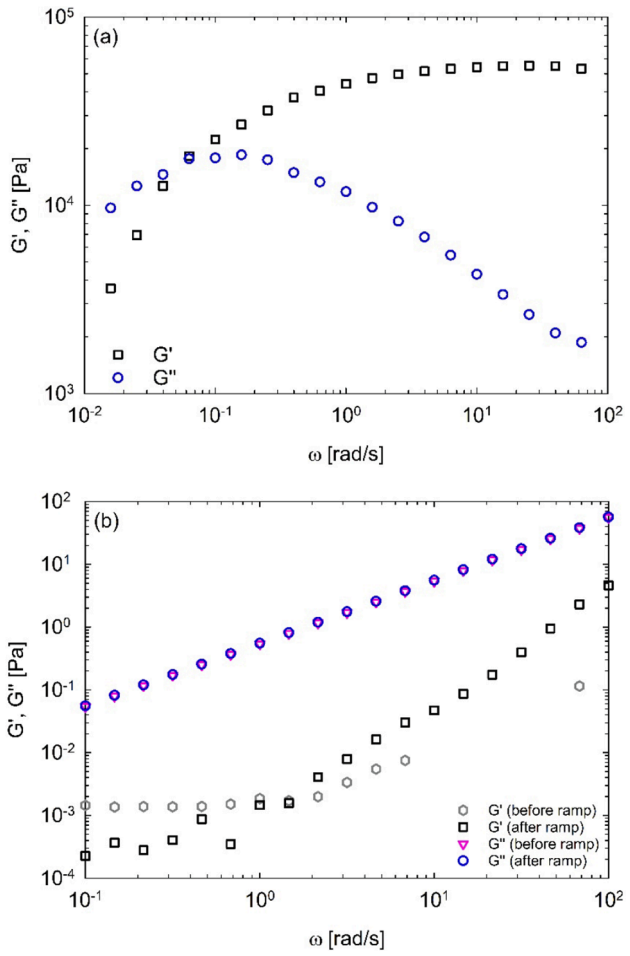

Fig. 6. Linear frequency responses of the 45 wt% Pluronic F68 water solution with 50 mM diclofenac sodium: (a) at 70 °C; (b) at 5 °C (before and after the ramp test).

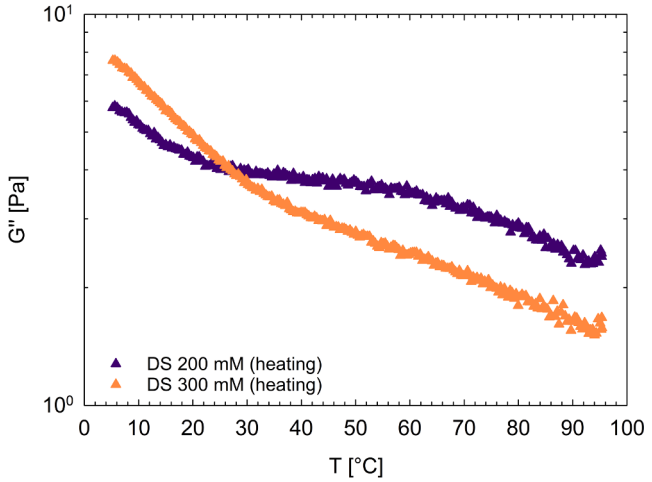

Fig. 7. Loss modulus vs temperature for the 45 wt% Pluronic F68 aqueous solutions with 200 and 300 mM diclofenac sodium (indicated with DS in the legend). Ramp rate equal to 5 °C/min.

any liquid-to-solid transition. This means that a significant amount of diclofenac sodium kills the Pluronic ability of self-assembling in a polar environment. In addition, no turbidity was macroscopically visible in the entire range of temperature, suggesting that the diclofenac is stable in the Pluronic solution at such a high concentration (about five times its solubility limit in water (Ledwidge and Corrigan, 1998)). We report in SI a movie of the visual microstructure of the 300 mM diclofenac sodium sample, where drug aggregates – clearly evident at low temperatures – reduce in size during heating and do not appear again during cooling, due to the drug solubility enhancement guaranteed by the physical interaction between the Pluronic and drug molecules.

It is worth plotting the diclofenac sodium concentration vs $1/T_T$ as shown in Fig. 8. The linear regression in Fig. 8

$$c_{DS} = c_0 - \frac{m}{T_T} \tag{7}$$

presents two fitting parameters, c_0 and m, which are equal to 204 ± 9 mM, and 5773 ± 311 °C·mM, respectively. c_0 represents the diclofenac sodium concentration above which no phase transition can be observed (obtained for $T_T \to \infty$). This is confirmed by the results of Fig. 7, showing the rheological behavior of the samples with 200 mM and 300 mM diclofenac sodium, which indeed does not show phase transitions. Eq. (7) represents an example of a predictive tool for evaluating the transition temperatures of drug delivery systems. It also allows computing the amount of drug to be added to the biomedical carrier to obtain the desired transition temperature.

3.2. NMR structure

High-resolution ^{1}H NMR spectra of diclofenac dissolved in pure D_2O (with no Pluronic) and in the presence of Pluronic F68, acquired at 25 °C, are shown in Fig. 9 and SI1 together with line assignments. A reference sample of diclofenac dissolved in D_2O is used to study the interactions between Pluronic molecules and the drug. Substantial changes were observed in the local environment of several diclofenac protons within the micellar system, compared with the pure D_2O solution. These mainly concern the shielding of the H5, H3, H7, H4 and H(6, 6′) protons. These chemical shift variations are indicative of drug-polymer interactions, responsible for drug solubilization in the micellar system. A strong overlap of the DS protons CH_2(1) with the PEO/PPO signals is also observed (Figure SI2). Furthermore, increasing drug concentration up to 300 mM causes further upfield shift of all protons, and this change is more pronounced for protons H(6,6′), H7 and H4, presumably due to drug-drug interactions.

The ^{1}H spectra of both preparations, acquired at the lowest temperature 5 °C, are characterized by the broadening of all diclofenac signals, which become well resolved with increasing temperature up to 25 °C and above (see Fig. SI3).

As temperature increases beyond the phase transition, pluronic-

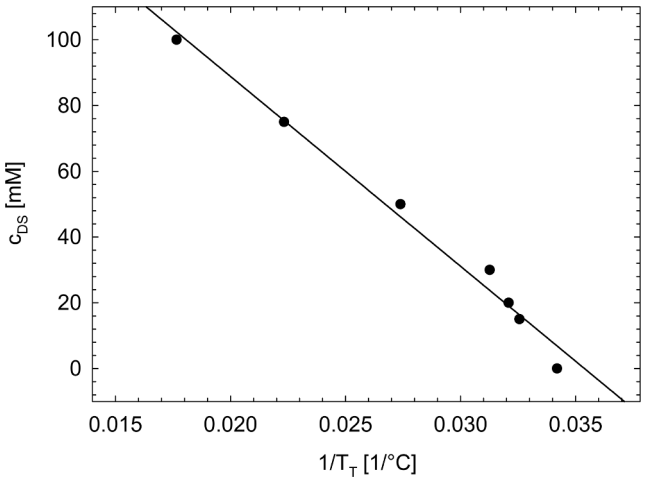

Fig. 8. Diclofenac sodium concentration vs $1/T_T$. The solid black line is the linear regression, following Eq. (7).

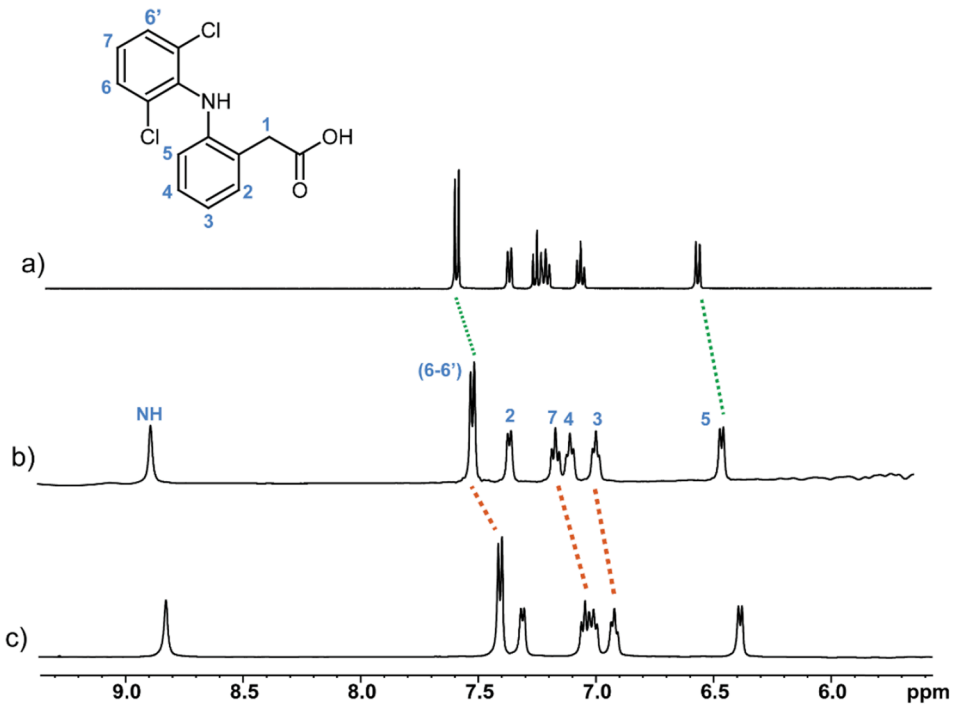

Fig. 9. ^{1}H HR NMR spectra (expanded aromatic region) of diclofenac sodium dissolved in: a) D_2O 15 mM, b) Pluronic F68/water 100 mM, c) Pluronic F68/water 300 mM acquired at 25 °C. Diclofenac chemical structure is also reported.

diclofenac (100 mM) samples become a more solid-like material, with limited conformational degrees of freedom and accordingly with an increase in residual dipolar couplings leading to extremely broadened signals. Consequently, experiments were performed using the HR-MAS set-up to obtain high-resolution spectra. The HR-MAS spectrum (see Fig. SI4) shows well resolved resonances for all species and no chemical shift variations are observed for the free drug/polymer in the solid phase compared with liquid sample. This accounts for a liquid water/polymer component freely dispersed in the solid-like phase, which is not observed in the high-resolution MAS spectrum. The drug molecules show well resolved lines as being dissolved within this hydrophilic/hydrophobic liquid fraction. The continuous presence of a liquid fraction was also observed over the entire phase diagram for aqueous solutions of Pluronic F-127 (Shaikhullina, 2020).

Useful information for the assessment of drug-polymer interactions can be obtained by 2D NMR ^{1}H–^{1}H correlation spectroscopy based on the nuclear Overhauser enhancement effect (NOE) (Castiglione, 2011). The 2D NOESY spectra of diclofenac sodium in Pluronic F68/H_2O solution (100 mM), acquired in a range of temperatures 5–25 °C, all exhibited negative NOE (characterized by the same phase as the diagonal) indicative of intermolecular interactions. The data, shown in Fig. 10, are acquired at the lowest temperature of 5 °C, when Pluronic

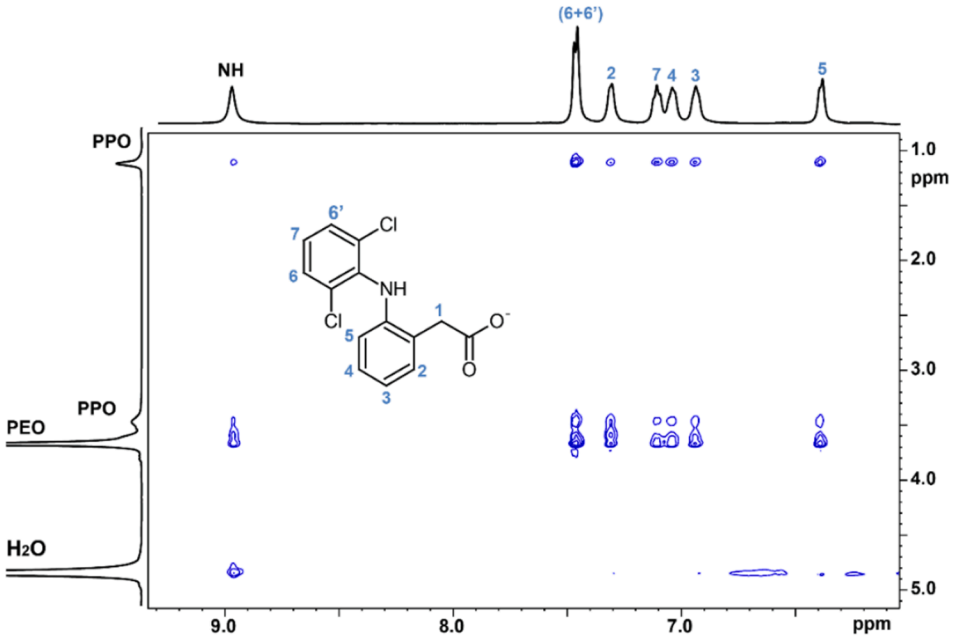

Fig. 10. ^{1}H–^{1}H NOESY spectrum of diclofenac sodium (100 mM) in Pluronic F68 acquired at 5 °C and 300 ms mixing time.

molecules and drug are in solution. Although the 2D map shows a strong overlap of the CH_2 (1) protons of the drug with PEO/PPO CH_2 signals, NOEs cross peaks are observed between all drug protons and PPO (methyl)/PEO (CH_2) of the polymer. In contrast, at higher temperatures 15–25 °C (see Fig. SI5), only the PPO methyl signal gives detectable cross peaks with the drug, revealing interactions between only the hydrophobic part of the polymer and the aromatic groups of the drug. These results indicate incorporation of drug molecules into the core of the spherical micelles, whereas the shell characterized by PEO is less filled with the drug.

Furthermore, by increasing the drug concentration up to 300 mM in Pluronic F68/H_2O solution and over the entire range of temperature investigated (see Fig. SI6), intense NOEs cross peaks are observed between all drug protons and PPO (methyl)/PEO (CH_2) of the polymer. These results indicate the presence of free drug molecules interacting indiscriminately with both PPO/PEO polymer blocks.

3.3. NMR diffusion

3.3.1. Analysis of water diffusion in neat F68 samples

We begin our discussion by considering the results obtained for water diffusion in Pluronic samples. Table 1 collects the self-diffusion coefficients of water at different temperatures, obtained either by fitting signal decay with a single Gaussian ($D_{G,wat}$), or with multiple Gaussian functions, via deconvolution ($D_{P,wat}$).

In both cases, the water diffusion coefficients in F68 samples were one order of magnitude smaller than those of pure liquid at similar temperatures ($2.597 \cdot 10^{-9}$ m^2/s for water at 30 °C (Tofts, 2000; Holz et al., 2000). This outcome was expected, considering the viscosity of the F68 solution, compared to that of pure water. Fig. 11a displays the diffusion coefficients obtained by means of the two approaches. Overall, the two profiles closely matched up to 25 °C, with the logarithm of the diffusion coefficient linearly increasing with temperature. The change in slope, taking place between 25 °C and 35 °C, can be associated to the liquid-to-solid transition, according to our previous results (see Figs. 3 and 4). Further increasing the temperature above 35 °C restored the initial trend, albeit with differences between $D_{G,wat}$ and $D_{P,wat}$ values.

To further investigate this outcome, we reported in Fig. 11b the PDFs obtained from Gaussian deconvolution and used to calculate the $D_{P,wat}$ values.

Prior discussing them, we briefly summarize some of the leading concepts underlying the application of Gaussian deconvolution. According to Eq. (6), a pure Gaussian diffusive process generates an infinitely narrow PDF (mathematically, a δ function) centred at a single diffusion coefficient, e.g., $D_{P,wat} = D$. Although this outcome is never observed in practice, the PDF for species diffusing in a homogeneous and isotropic medium can still be expected to be essentially unimodal, e.g. with values distributed around a single maximum. Conversely, the presence of multiple peaks may be associated with the existence of groups of molecules experiencing widely different chemical, or physical, environments. The former may be associated with the establishment of strong intermolecular interactions between the diffusing species and the medium, while the latter with the presence of molecular structures (such as networks or supramolecular assemblies) hindering diffusion. Some effect on the observed PDF can likely be expected when the time scale at which diffusion is probed is comparable with that of the above phenomena.

It is important to note that the PDF obtained from NMR data often displays some residual weights which, apparently, are not representative of molecular diffusion, but involve other factors, such as instrumental data noise. We are currently working on the approaches that will help us decoupling the contribution of such factors. Meanwhile, in the present work, we chose to focus on the most representative portion of the PDF, in order to appropriately describe our results. Since all the PDFs considered are unimodal, we chose the value of D_P as that associated to the largest weight in the PDF (see the SI for a detailed discussion on this topic).

Coming back to our results, the increase of medium viscosity and heterogeneity associated with micelles aggregation may well set up a physical barrier to free water diffusion and explain the decrease of the diffusion coefficient across the liquid-to-solid transition. Yet, the absence of significant changes in the PDFs reported in Fig. 11b indicates that, on the time scale probed by our experiments (10–100 ms), the diffusing medium was essentially isotropic with respect to water diffusion. At present, the change in PDF broadening across the transition has no clear explanation. Further investigations will be necessary to clarify this outcome.

The uncertainties reported in Fig. 11a for Gaussian deconvolution (defined in the SI), are consistent with the width of the distributions in Fig. 11b, and greater than those obtained by means of single-Gaussian fitting, below the phase transition. Above this point, the PDFs appear very sharp, with correspondingly lower uncertainties.

3.3.2. Analysis of drug and water diffusion in pluronic-drug samples

The diffusion of water and diclofenac sodium was subsequently investigated in Pluronic solutions containing diclofenac at two different concentrations. As discussed above (see Figs. 4 and 6), the addition of diclofenac sodium markedly affected the F68 thermal behavior. Table 2 collects the results obtained for water and diclofenac sodium in F68 samples in the presence of the drug at 100 mM concentration.

Fig. 12 summarizes our results for water diffusion. The values of $D_{G,wat}$ and $D_{P,wat}$ were similar at all temperatures. The diffusion coefficient increased up to 35 °C, to decrease at 70 °C, beyond the liquid-to-solid transition temperature detected for F68 (see above). As in drug-free samples (see above), no specific feature emerged during PDF analysis, thereby suggesting that water diffusion was essentially free and unrestricted at all temperatures investigated. Also in this case, the drop of water diffusion coefficient at high temperature can be associated with the increase in medium viscosity brought by the phase transition.

The results for diclofenac sodium diffusion are displayed in Fig. 13. The logarithms of $D_{G,drug}$ and $D_{P,drug}$ monotonically increased with temperature. Both approaches provided comparable results at all temperatures, thereby suggesting drug diffusion to follow the Gaussian model.

The PDFs reported in Fig. 13 are unimodal and show no evidence of distinct diffusive regimes within the temperature range investigated. The presence of left-extending tails at low temperature (5 and 15 °C) may possibly be associated with the drug-polymer interactions evidenced by the 2D NOESY data analysis and appears to be the main reason for the larger uncertainty of the associated diffusion coefficients. At present, it is difficult to assess whether these features are associated with drug-unimer or drug-micelle interactions. The latter is less likely, due to the fact PDF tails disappear by increasing the temperature.

Now we turn our attention to the NMR measurements performed on the 300 mM sample. Our results are summarized in Table 3. According to our rheological data (see Fig. 7), no significant micelle formation, nor a liquid-to-solid transition, was detected in the range between 5 and 95 °C for this sample. In line with these outcomes, the water diffusion coefficient profiles, depicted in Fig. 14, do not show drastic changes with temperature. $D_{G,wat}$ and $D_{P,wat}$ values were similar at almost all

Table 1
Diffusion coefficients of water in neat F68 samples at different temperatures, obtained by means of standard regression ($D_{G,wat}$) and Gaussian deconvolution ($D_{P,wat}$). Significant digits are reported to within the standard deviations given in parentheses.

T [°C]	$D_{G,wat}$ [m^2/s]	$D_{P,wat}$ [m^2/s]
5	$2.202(6)\cdot10^{-10}$	$2.2(2)\cdot10^{-10}$
15	$3.34(2)\cdot10^{-10}$	$3.3(6)\cdot10^{-10}$
25	$5.18(2)\cdot10^{-10}$	$5.1(9)\cdot10^{-10}$
35	$4.9(2)\cdot10^{-10}$	$5.89(3)\cdot10^{-10}$
45	$7.1(2)\cdot10^{-10}$	$8.47(5)\cdot10^{-10}$

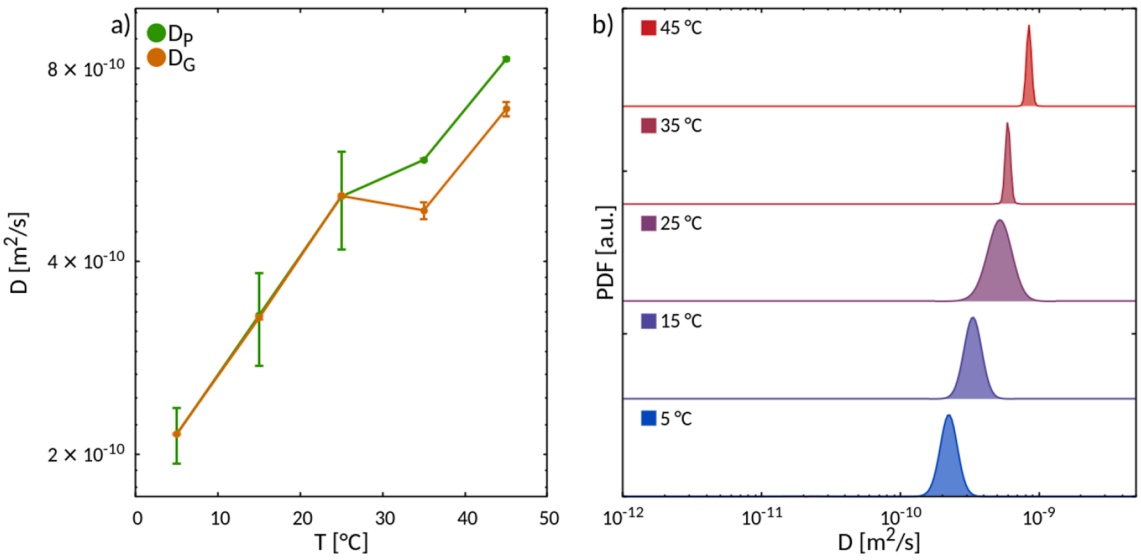

Fig. 11. A) logarithmic plot of water diffusion coefficients in f68 samples plotted against temperature. standard deviations are also reported (seeTable 1); b) Normalized probability distribution functions for water obtained from Gaussian deconvolution.

Table 2
Diffusion coefficients of water and diclofenac sodium in drug-loaded (diclofenac 100 mM) F68 samples at different temperatures, obtained by means of standard regression (D_G) and Gaussian deconvolution (D_P). Significant digits are reported to within the standard deviations, given in parentheses.

T [°C]	$D_{G,wat}$ [m^2/s]	$D_{P,wat}$ [m^2/s]	$D_{G,drug}$ [m^2/s]	$D_{P,drug}$ [m^2/s]
5	$1.91(2)\cdot10^{-10}$	$2.0(2)\cdot10^{-10}$	$2.80(3)\cdot10^{-12}$	$3(2)\cdot10^{-12}$
15	$3.12(5)\cdot10^{-10}$	$3.4(8)\cdot10^{-10}$	$6.23(8)\cdot10^{-12}$	$7(3)\cdot10^{-12}$
25	$4.33(2)\cdot10^{-10}$	$4.4(5)\cdot10^{-10}$	$1.52(1)\cdot10^{-11}$	$1.4(4)\cdot10^{-11}$
35	$7.13(7)\cdot10^{-10}$	$7.2(8)\cdot10^{-10}$	$2.57(2)\cdot10^{-11}$	$2.7(3)\cdot10^{-11}$
70	$5.8(2)\cdot10^{-10}$	$6.3(6)\cdot10^{-10}$	$9.9(2)\cdot10^{-11}$	$1.2(3)\cdot10^{-10}$

temperatures. This observation, along with the unimodal character of the PDFs, supports the applicability of a Gaussian diffusion model up to 45 °C, where different estimates were obtained. Here, the PDF shows a thin left-extending tail, whose origin must be be clarified. Conversely, the increased $D_{P,wat}$ uncertainty is likely to be related to PDF broadening.

The results for diclofenac sodium are reported in Fig. 15. The differences between $D_{G,drug}$ and $D_{P,drug}$ estimates were significant at 5 °C, consistently with the PDF shape at this temperature (see Fig. 15a). The remaining PDFs, also unimodal, display small left-extending tails at almost all temperatures. According to NOESY data analysis (see the Figures in the SI), these tails may tentatively be associated to the strong interactions taking place between drug protons and PPO (methyl)/PEO (CH_2) groups in this sample. Clearly, in such cases, the Gaussian diffusion model may not adequately describe solute diffusion, and alternative models must be considered.

4. Conclusions

The phase transitions and structural characteristics of aqueous solutions of Pluronic F68 and diclofenac sodium were studied by means of rheology and NMR. Water solutions with a fixed Pluronic F68 concentration and various diclofenac sodium amounts were prepared. The pluronic-drug systems were analyzed through temperature ramp tests at

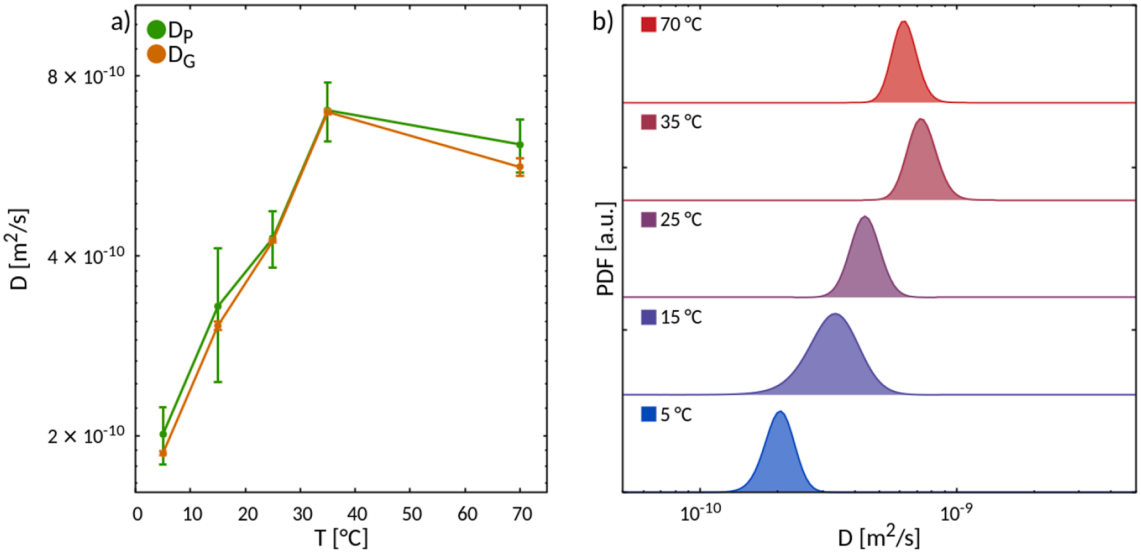

Fig. 12. A) logarithmic plot of water diffusion coefficients in drug-loaded (diclofenac 100 mM) F68 samples, plotted against temperature. Standard deviations are also reported (see Table 2); b) Normalized probability distribution functions for diclofenac obtained from Gaussian deconvolution.

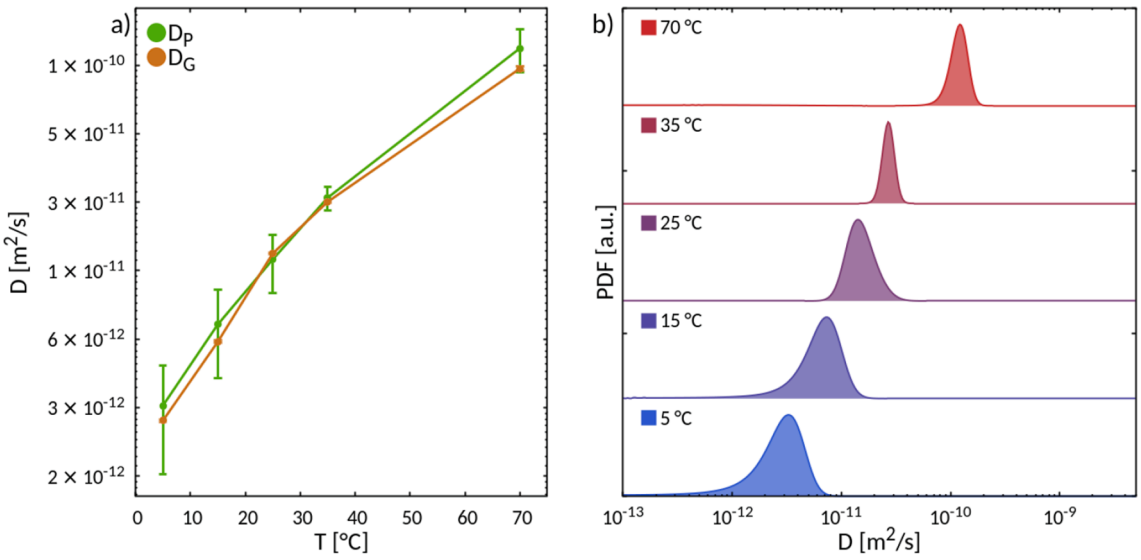

Fig. 13. A) logarithmic plot of diclofenac diffusion coefficients in drug-loaded (diclofenac 100 mM) F68 samples, plotted against temperature. Standard deviations are also reported (see Table 2); b) Normalized probability distribution functions for diclofenac obtained from Gaussian deconvolution.

Table 3
Diffusion coefficients of water and diclofenac sodium in drug-loaded (diclofenac 300 mM) F68 samples at different temperatures, obtained by means of standard regression (D_G) and Gaussian deconvolution (D_P). Significant digits are reported to within the standard deviations, given in parentheses.

T [°C]	$D_{G,wat}$ [m^2/s]	$D_{P,wat}$ [m^2/s]	$D_{G,drug}$ [m^2/s]	$D_{P,drug}$ [m^2/s]
5	$1.59(1)\cdot10^{-10}$	$1.7(2)\cdot10^{-10}$	$2.06(2)\cdot10^{-12}$	$3(4)\cdot10^{-12}$
15	$3.267(4)\cdot10^{-10}$	$3.2(4)\cdot10^{-10}$	$4.58(3)\cdot10^{-12}$	$5(2)\cdot10^{-12}$
25	$4.95(2)\cdot10^{-10}$	$5.0(5)\cdot10^{-10}$	$1.043(3)\cdot10^{-11}$	$1.1(3)\cdot10^{-11}$
35	$6.70(9)\cdot10^{-10}$	$6.9(8)\cdot10^{-10}$	$2.026(7)\cdot10^{-11}$	$2.1(4)\cdot10^{-11}$
45	$7.26(29)\cdot10^{-10}$	$9(3)\cdot10^{-10}$	$2.68(6)\cdot10^{-11}$	$3(1)\cdot10^{-11}$

two different ramp rates, namely, 5 and 0.5 °C/min, in order to detect the morphological transitions upon heating and cooling cycles. Reversible liquid-to-solid transitions were observed, and an experimental phase diagram was obtained for the 45 wt% Pluronic solutions with a drug content ranging between 0 mM and 100 mM. The transition temperature was found to increase with increasing diclofenac sodium concentration. Two different rheological properties were identified according to temperature range and diclofenac concentration – before and after the transition temperature. A similar behaviour has been widely described in literature for the system without drug, where the solid response has been assigned to a BCC structure.

At diclofenac sodium concentrations above 200 mM, no phase transition was detected in the corresponding temperature range, as also confirmed by the diffusion coefficient profiles. Although we do not have a definitive explanation of such behaviour, we can speculate that in the presence of a significant amount of diclofenac molecules the formation of self-assembled aggregates is hindered, or that their amount does not reach a critical number to induce a phase transition. Ongoing studies will shed a light on the definitive mechanisms for the absence of such a transition. It is undeniable that Pluronic molecules serve as support for diclofenac solubility, allowing for homogeneous solution at a concentration five times higher than the diclofenac sodium solubility in pure water. An optical rheometrical investigation has also proven that the drug dissolution is irreversible on the experimental time scale. This

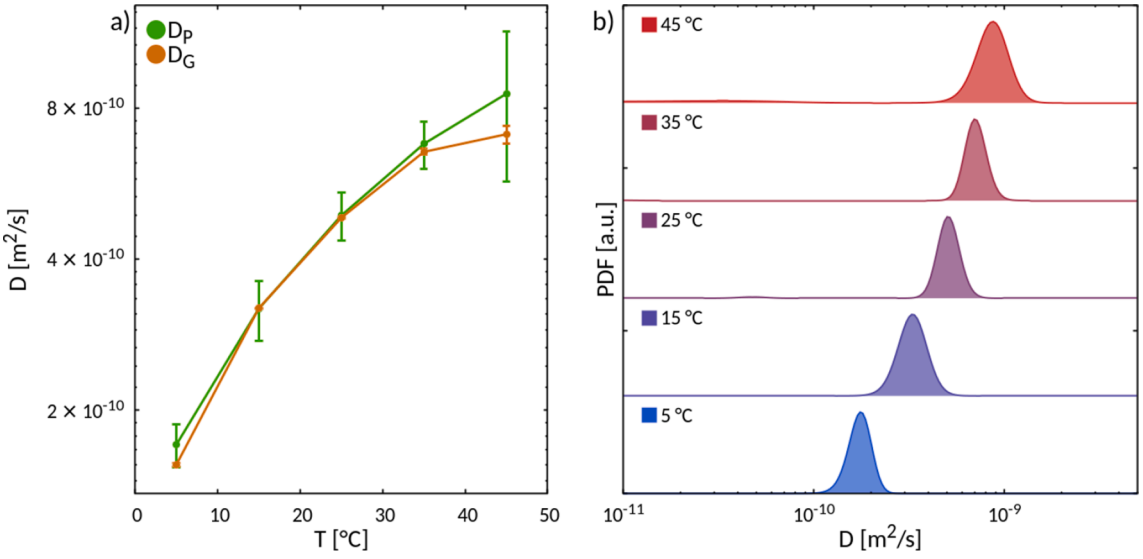

Fig. 14. A) logarithmic plot of water diffusion coefficients in drug-loaded (diclofenac 300 mM) F68 samples, plotted against temperature. Standard deviations are also reported (see Table 3); b) Normalized probability distribution functions for diclofenac obtained from Gaussian deconvolution.

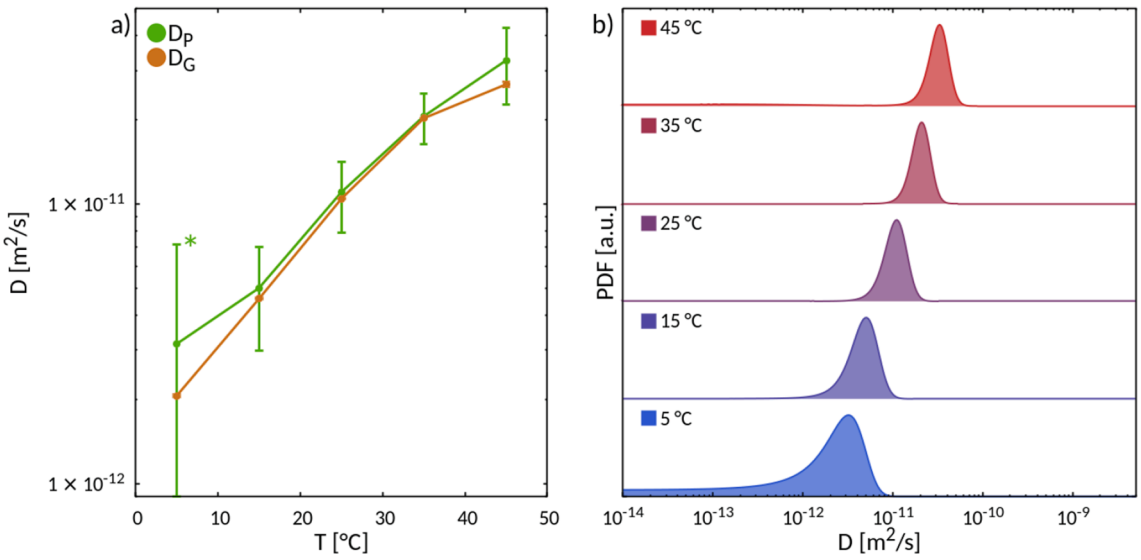

Fig. 15. A) logarithmic plot of diclofenac diffusion coefficients in drug-loaded (diclofenac 300 mM) F68 samples, plotted against temperature. Standard deviations are also reported (see Table 3). *) For clarity, the standard deviation of this distribution is only partially shown; b) Normalized probability distribution functions for diclofenac obtained from Gaussian deconvolution.

result can be useful for enhancing the solubility of any kind of hydrophobic molecules in colloidal self-assemblies.

NMR results, as well as the water and drug diffusion coefficient profiles, confirm the existence of a liquid to solid transition for systems with a drug content lower than 100 mM, with no chemical shift variations for both Pluronic and diclofenac molecules, indicating the presence of only physical interactions between the two entities, even at high temperatures, which explains the temperature reversibility. The 2D NOESY spectra of diclofenac sodium in Pluronic F68/H_2O solution reveals that the drug interacts with both PEO and PPO at low temperatures, whereas at high temperatures only interactions between the hydrophobic part of the polymer and the aromatic groups of the drug are clear. This means that with increasing temperature the PPO and the drug hydrophilicities probably worsen, bringing to a stronger interaction between the two molecules, and a consequent more crowded micellar core. The comparison of diffusion coefficients obtained by means of standard regression and Gaussian deconvolution revealed no significant deviations from the ordinary Gaussian diffusion model for water and diclofenac. No evidence of distinct diffusive regimes emerged during PDF analysis, thus supporting the idea that the diffusing medium was perceived as essentially homogeneous by PGSE-NMR experiments. Nevertheless, the presence of reproducible, yet unexplained, anomalies in drug displacement distribution at low temperatures suggests that Gaussian deconvolution is sensitive to the interactions between the probed species and their surrounding environment. Although additional efforts will be necessary to fine tune results interpretation, we note that, to our knowledge, this approach has never been applied to model raw PGSE-NMR data. We believe the results we have obtained so far are encouraging, and prompt us to further develop this technique.

In conclusion, the combination of complementary experimental techniques was able to fully characterize a potentially viable drug-delivery system. This strategy appears promising in identifying candidates suitable for various drug-delivery applications.

Declaration of Competing Interest

The authors declare that they have no known competing financial interests or personal relationships that could have appeared to influence the work reported in this paper.

Data availability

Data will be made available on request.

Appendix A. Supplementary material

Supplementary data to this article can be found online at https://doi.org/10.1016/j.ijpharm.2023.123353.

References

Alexandridis, P., Holzwarth, J.F., Alan Hatton, T., 1994. Micellization of poly (ethylene oxide)-poly (propylene oxide)-poly (ethylene oxide) triblock copolymers in aqueous solutions: thermodynamics of copolymer association. Macromolecules 27 (9), 2414–2425.

Alexandridis, P., Zhou, D., Khan, A., 1996. Lyotropic liquid crystallinity in amphiphilic block copolymers: temperature effects on phase behavior and structure for poly (ethylene oxide)-b-poly (propylene oxide)-b-poly (ethylene oxide) copolymers of different composition. Langmuir 12 (11), 2690–2700.

Artzner, F., et al., 2007. Interactions between poloxamers in aqueous solutions: micellization and gelation studied by differential scanning calorimetry, small angle X-ray scattering, and rheology. Langmuir 23 (9), 5085–5092.

Basak, R., Bandyopadhyay, R., 2013. Encapsulation of hydrophobic drugs in Pluronic F127 micelles: effects of drug hydrophobicity, solution temperature, and pH. Langmuir 29 (13), 4350–4356.

Batrakova, E.V., Kabanov, A.V., 2008. Pluronic block copolymers: evolution of drug delivery concept from inert nanocarriers to biological response modifiers. J. Control. Release 130 (2), 98–106.

Bedrov, D., Ayyagari, C., Smith, G.D., 2006. Multiscale modeling of poly (ethylene oxide)– poly (propylene oxide)– poly (ethylene oxide) triblock copolymer micelles in aqueous solution. J. Chem. Theory Comput. 2 (3), 598–606.

Bertz, A., et al., 2013. Mobility of Green Fluorescent Protein in Hydrogel-Based Drug-Delivery Systems Studied by Anisotropy and Fluorescence Recovery After Photobleaching. Macromol. Biosci. 13 (2), 215–226.

Biondi, M., et al., 2008. Controlled drug delivery in tissue engineering. Adv. Drug Deliv. Rev. 60 (2), 229–242.

Bodratti, A.M., Alexandridis, P., 2018. Formulation of poloxamers for drug delivery. J. Functional Biomater. 9 (1), 11.

Callaghan, P.T., Eccles, C.D., Xia, Y., 1988. NMR microscopy of dynamic displacements: k-space and q-space imaging. J. Phys. E Sci. Instrum. 21 (8), 820.

Casalegno, M., Ferro, M., Rossi, F., Raos, G., Mele, A., 2019. Evidence of superdiffusive nanoscale motion in anionic polymeric hydrogels: Analysis of PGSE- NMR data and comparison with drug release properties. J. Control. Release 305. https://doi.org/10.1016/j.jconrel.2019.05.027.

Castiglione, F., et al., 2011. Selective interaction of 2, 6-di-O-methyl-β-cyclodextrin and Pluronic F127 micelles leading to micellar rupture: a nuclear magnetic resonance study. J. Phys. Chem. B 115 (29), 9005–9013.

Chakraborty, I., et al., 2019. Nanoparticle mobility over a surface as a probe for weak transient disordered peptide–peptide interactions. Nano Lett. 19 (9), 6524–6534.

Chen, J., et al., 2013. Mechanical, rheological and release behaviors of a poloxamer 407/poloxamer 188/carbopol 940 thermosensitive composite hydrogel. Molecules 18 (10), 12415–12425.
Chubinskaya, S., et al., 2019. Agili-C implant promotes the regenerative capacity of articular cartilage defects in an ex vivo model. Knee Surg. Sports Traumatol. Arthrosc. 27, 1953–1964.
Chung, J.Y., et al., 2014. Comparison of articular cartilage repair with different hydrogel-human umbilical cord blood-derived mesenchymal stem cell composites in a rat model. Stem Cell Res Ther 5, 1–13.
Clincke, M.-F., et al., 2011. Effect of surfactant pluronic F-68 on CHO cell growth, metabolism, production, and glycosylation of human recombinant IFN-γ in mild operating conditions. Biotechnol. Prog. 27 (1), 181–190.
Cohen, Y., Assaf, Y., 2002. High b-value q-space analyzed diffusion-weighted MRS and MRI in neuronal tissues–a technical review. NMR in Biomed.: Int. J. Devoted Develop. Application Magn. Resonance In Vivo 15 (7-8), 516–542.
Cory, D.G., Garroway, A.N., 1990. Measurement of translational displacement probabilities by NMR: an indicator of compartmentation. Magn. Reson. Med. 14, 435–444.
Costanzo, S., et al., 2021. Rheology and morphology of Pluronic F68 in water. Phys. Fluids 33 (4), 043113.
Denkova, A.G., et al., 2011. Complex morphologies of self-assembled block copolymer micelles in binary solvent mixtures: the role of solvent–solvent correlations. Soft Matter 7 (14), 6622–6628.
Dorn, Klaus, Hoerpel, Gerhard, Ringsdorf, Helmut, 1985. Polymeric antitumor agents on a molecular and cellular level. Bioactive Polymeric Systems: An Overview 531–585.
Dumortier, G., et al., 2006. A review of poloxamer 407 pharmaceutical and pharmacological characteristics. Pharm. Res. 23, 2709–2728.
Fick, A., 1855. Ueber diffusion. Ann. Phys. 170 (1), 59–86.
Fiorati, A., et al., 2020. TEMPO-Nanocellulose/Ca2+ Hydrogels: Ibuprofen Drug Diffusion and In Vitro Cytocompatibility. Materials 13 (1), 183.
Gaisford, S., Beezer, A.E., Mitchell, J.C., 1997. Diode-array UV spectrometric evidence for cooperative interactions in binary mixtures of pluronics F77, F87, and F127. Langmuir 13 (10), 2606–2607.
Gioffredi, E., et al., 2016. Pluronic F127 hydrogel characterization and biofabrication in cellularized constructs for tissue engineering applications. Procedia Cirp 49, 125–132.
Gjerde, N., et al., 2018. Effect of PCL end-groups on the self-assembly process of Pluronic in aqueous media. Phys. Chem. Chem. Phys. 20 (4), 2585–2596.
Gnuplot release 5.4. Thomas Williams and Colin Kelley. Gnuplot 5.4: An Interactive Plotting Program. http://sourceforge.net/projects/gnuplot (last accessed: 01/03/2023).
Guan, J., Wang, B.o., Granick, S., 2014. Even hard-sphere colloidal suspensions display Fickian yet non-Gaussian diffusion. ACS Nano 8 (4), 3331–3336.
Herzberger, J., et al., 2016. Polymerization of ethylene oxide, propylene oxide, and other alkylene oxides: synthesis, novel polymer architectures, and bioconjugation. Chem. Rev. 116 (4), 2170–2243.
Holz, M., Heil, S.R., Sacco, A., 2000. Temperature-dependent self-diffusion coefficients of water and six selected molecular liquids for calibration in accurate 1H NMR PFG measurements. Phys. Chem. Chem. Phys. 2 (20), 4740–4742.
Kim, M., et al., 2018. Comparison of in vivo targeting ability between cRGD and collagen-targeting peptide conjugated nano-carriers for atherosclerosis. J. Control. Release 269, 337–346.
Kurtuldu, Hüseyin, et al. "Enhancement of biomixing by swimming algal cells in two-dimensional films." Proceedings of the National Academy of Sciences 108.26 (2011): 10391-10395.
Ledwidge, M.T., Corrigan, O.I., 1998. Effects of surface active characteristics and solid state forms on the pH solubility profiles of drug–salt systems. Int. J. Pharm. 174 (1-2), 187–200.
Levenberg, K., 1944. A Method for the Solution of Certain Problems in Least Squares. Quart. Appl. Math. 2, 164–168.
Liu, Y.u., et al., 2007. Controlled delivery of recombinant hirudin based on thermo-sensitive Pluronic® F127 hydrogel for subcutaneous administration: In vitro and in vivo characterization. J. Control. Release 117 (3), 387–395.
Lucy, L.B., 1974. An iterative technique for the rectification of observed distributions. Astron. J. 79, 745.
Marquardt, D., 1963. An Algorithm for Least-Squares Estimation of Nonlinear Parameters. SIAM J. Appl. Math. 11, 431–441.
Meng, Y., et al., 2006. A family of highly ordered mesoporous polymer resin and carbon structures from organic− organic self-assembly. Chem. Mater. 18 (18), 4447–4464.
Mohammadi, M.R., et al., 2017. Nanomaterials engineering for drug delivery: a hybridization approach. J. Mater. Chem. B 5 (22), 3995–4018.
Mortensen, K., 2001. Structural studies of lamellar surfactant systems under shear. Curr. Opin. Colloid Interface Sci. 6 (2), 140–145.
Müller, M., et al., 2015. Nanostructured Pluronic hydrogels as bioinks for 3D bioprinting. Biofabrication 7 (3), 035006.
Newman, M.J., Balusubramanian, M., Todd, C.W., 1998. Development of adjuvant-active nonionic block copolymers. Adv. Drug Deliv. Rev. 32 (3), 199–223.
Oshiro, A., et al., 2014. Pluronics f-127/l-81 binary hydrogels as drug-delivery systems: influence of physicochemical aspects on release kinetics and cytotoxicity. Langmuir 30 (45), 13689–13698.
Pasquino, R., et al., 2019. An experimental rheological phase diagram of a tri-block co-polymer in water validated against dissipative particle dynamics simulations. Soft Matter 15 (6), 1396–1404.
Quintans-Júnior, L.J., et al., 2018. Nanoemulsion thermoreversible pluronic F127-based hydrogel containing Hyptis pectinata (Lamiaceae) leaf essential oil produced a lasting anti-hyperalgesic effect in chronic noninflammatory widespread pain in mice. Mol. Neurobiol. 55, 1665–1675.
Rahdar, A., Kazemi, S., Askari, F., 2018. Pluronic as nano-carrier platform for drug delivery systems. Nanomed. Res. J. 3, 174–179.
Ray, D., Kohlbrecher, J., Aswal, V.K., 2017. Effect of ionic surfactant on the self-assembly of triblock copolymer. AIP Conference Proceedings. Vol. 1832. No. 1. AIP Publishing LLC, 2017.
Richardson, W.H., 1972. Bayesian-Based Iterative Method of Image Restoration. J. Opt. Soc. Am. 62 (1), 55–59.
Russo, J., Fiegel, J., Brogden, N.K., 2020. Rheological and drug delivery characteristics of poloxamer-based diclofenac sodium formulations for chronic wound site analgesia. Pharmaceutics 12 (12), 1214.
Russo, J., Fiegel, J., Brogden, N.K., 2022. Effect of Salt Form on Gelation and Drug Delivery Properties of Diclofenac-Loaded Poloxamer Gels for Delivery to Impaired Skin. Pharm. Res. 39 (10), 2515–2527.
Sahu, A., et al., 2011. Encapsulation of curcumin in Pluronic block copolymer micelles for drug delivery applications. J. Biomater. Appl. 25 (6), 619–639.
Salerno, A., Netti, P.A., 2021. Review on computer-aided design and manufacturing of drug delivery scaffolds for cell guidance and tissue regeneration. Front. Bioeng. Biotechnol. 9, 682133.
Saveyn, P., et al., 2009. Solubilization of flurbiprofen within non-ionic Tween 20 surfactant micelles: a 19 F and 1H NMR study. Phys. Chem. Chem. Phys. 11 (26), 5462–5468.
Sayed, M., 2021. Pal, Haridas "An overview from simple host–guest systems to progressively complex supramolecular assemblies". Phys. Chem. Chem. Phys. 23, 26085–26107.
Scherlund, M., Brodin, A., Malmsten, M., 2000. Micellization and gelation in block copolymer systems containing local anesthetics. Int. J. Pharm. 211 (1-2), 37–49.
Schmolka, I.R., 1972. Artificial skin I. Preparation and properties of pluronic F-127 gels for treatment of burns. J. Biomed. Mater. Res. 6 (6), 571–582.
Scholer, D.W., et al., 1986. Pharmacology of diclofenac sodium. Am. J. Med. 80 (4), 34–38.
Shaikhullina, M., et al., 2020. NMR relaxation and self-diffusion in aqueous micellar gels of pluronic F-127. J. Mol. Liq. 306, 112898.
Sharma, P.K., Bhatia, S.R., 2004. Effect of anti-inflammatories on Pluronic® F127: micellar assembly, gelation and partitioning. Int. J. Pharm. 278 (2), 361–377.
Smeraldo, A., et al., 2021. Tuning of Hydrogel Architectures by Ionotropic Gelation in Microfluidics: Beyond Batch Processing to Multimodal Diagnostics. Biomedicines 9 (11), 1551.
Stejskal, E.O., Tanner, J.E., 1965. Spin diffusion measurements: spin echoes in the presence of a time-dependent field gradient. J. Chem. Phys. 42 (1), 288–292.
Stempfle, B., et al., 2014. Anomalous diffusion in thermoresponsive polymer–clay composite hydrogels probed by wide-field fluorescence microscopy. Langmuir 30 (46), 14056–14061.
Suntornnond, R., et al., 2017. A highly printable and biocompatible hydrogel composite for direct printing of soft and perfusable vasculature-like structures. Sci. Rep. 7 (1), 1–11.
Tang, S., Wang, M., Olsen, B.D., 2015. Anomalous self-diffusion and sticky Rouse dynamics in associative protein hydrogels. J. Am. Chem. Soc. 137 (11), 3946–3957.
Thorneywork, A.L., et al., 2016. On the Gaussian approximation in colloidal hard sphere fluids. Soft Matter 12 (18), 4129–4134.
Tofts, P.S., et al., 2000. "Test liquids for quantitative MRI measurements of self-diffusion coefficient in vivo." Magnetic Resonance in Medicine: An Official Journal of the International Society for. Magn. Reson. Med. 43 (3), 368–374.
Torchilin, V.P., 2001. Structure and design of polymeric surfactant-based drug delivery systems. J. Control. Release 73 (2-3), 137–172.
Wang, B.o., et al., 2012. When Brownian diffusion is not Gaussian. Nat. Mater. 11 (6), 481–485.
Wang, Bo, et al., 2009. Anomalous yet brownian. Proc. Natl. Acad. Sci. 106.36 (2009): 15160-15164.
Wanka, G., Hoffmann, H., Ulbricht, W., 1994. Phase diagrams and aggregation behavior of poly (oxyethylene)-poly (oxypropylene)-poly (oxyethylene) triblock copolymers in aqueous solutions. Macromolecules 27 (15), 4145–4159.
Wu, Y.L., et al., 2006. Effect of salt on the phase behaviour of F68 triblock PEO/PPO/PEO copolymer. J. Phys. Condens. Matter 18 (19), 4461.
Wu, D.H., Chen, A.D., Johnson, C.S., 1995. An improved diffusion-ordered spectroscopy experiment incorporating bipolar-gradient pulses. J. Magn. Reson. A 115 (2), 260–264.
Yang, L., Alexandridis, P., 2000. Physicochemical aspects of drug delivery and release from polymer-based colloids. Curr. Opin. Colloid Interface Sci. 5 (1-2), 132–143.
Yong, C.S., et al., 2001. Effect of sodium chloride on the gelation temperature, gel strength and bioadhesive force of poloxamer gels containing diclofenac sodium. Int. J. Pharm. 226 (1-2), 195–205.
Zarrintaj, P., et al., 2017. Can regenerative medicine and nanotechnology combine to heal wounds? The search for the ideal wound dressing. Nanomedicine 12 (19), 2403–2422.
Zarrintaj, P., et al., 2018. Poloxamer-based stimuli-responsive biomaterials. Mater. Today:. Proc. 5 (7), 15516–15523.
Zarrintaj, P., et al., 2020. Poloxamer: A versatile tri-block copolymer for biomedical applications. Acta Biomater. 110, 37–67.
Zhang, Y., et al., 2010. A novel paclitaxel-loaded poly (ε-caprolactone)/Poloxamer 188 blend nanoparticle overcoming multidrug resistance for cancer treatment. Acta Biomater. 6 (6), 2045–2052.
Žilnik, L.F., et al., 2007. Solubility of sodium diclofenac in different solvents. Fluid Phase Equilib. 261 (1-2), 140–145.